Vol 16 No 9, September 2007
1009-1963/2007/16(09)/2737-08

Chinese Physics

© 2007 Chin. Phys. Soc.
and IOP Publishing Ltd

A method of designing photonic crystal grating slow-wave circuit for Ribbon–Beam microwave travelling wave amplifiers*

Yin Hai-Rong(殷海荣)†, Gong Yu-Bin(宫玉彬), Wei Yan-Yu(魏彦玉), Gong Hua-Rong(巩华荣), Yue Ling-Na(岳玲娜), Lu Zhi-Gang(路志刚), Huang Min-Zhi(黄民智), and Wang Wen-Xiang(王文祥)

School of Physical Electronics, University of Electronic Science and Technology of China, Chengdu 610005, *China*

(Received 5 November 2006; revised manuscript received 9 March 2007)

A method of designing a photonic crystal grating slow-wave circuit in which the cylinders of the 2D photonic crystals dot on a cross-sectional plane is established by calculating the band structures of the 2D photonic crystals, and the eigenfrequency of the equivalent waveguide grating. For calculating the band structures, the eigenvalue equations of the photonic crystals in the system of photonic crystal grating slow-wave circuit are derived in a special polarization mode. Two examples are taken to show the method. The design result is validated by the scattering parameters of the same circuit. The result indicates that there exists no photonic band gap if the metal gratings do not extend into the photonic crystals; the design of the circuit without the metal gratings extending into the photonic crystals is less flexible than that with the metal gratings extending into the photonic crystals.

Keywords: TWTs, photonic crystals, millimetre-wave, THz, slow-wave circuit
PACC: 4270Q, 5270G, 5235H

1. Introduction

Travelling wave amplifiers (TWAs) were discovered in the mid-twentieth century for radar applications,[1] which are traditionally employed to generate high-power radiation. A TWA acts as a wideband microwave amplifier. This wideband amplification feature is obtained by the use of an interaction circuit, commonly named slow-wave circuit, which essentially is a transmission line and usually without any resonant elements. Generally, a slow-wave circuit (SWC) is a kind of slow-wave structure (SWS) shielded by a metal waveguide. And there are lots of modes existing together. The existence of non-operating modes restricts the operating band-width, and may make the TWAs unstable. An SWC, in which only the operating mode can exist, is an ideal structure for TWA. But, there is no way to realize this notion until the concept of photonic crystals (PhCs)[2] is proposed.

PhCs are artificial materials with the capability of filtering electromagnetic waves (EMWs). If an SWS is enclosed entirely by a PhC, the non-operating modes have the opportunity to radiate outward through the PhC, rather than propagate along the SWC shielded by a waveguide. Without the competition with the undesired modes, the TWAs based on PhC SWCs can be designed to have a wider band-width, or lower operating voltage, or both; and be more stable.[3−5]

Theoretically, PhC SWC should be a three-layer configuration as shown in Fig.1, in which the PhC layers are outside for confining the desiring modes and sieving the others; In the middle there are an SWS layer for shaping waves with phase speeds slower than the speed of light in vacuum, and a beam tunnel for the electron beam to pass through. Sometimes, the layers of PhCs and SWS may be combined in practice; in such a case, the three-layer configuration is still available theoretically.

A photonic crystal grating SWC (PG-SWC) may be structured by using two-dimensional PhCs for the layer of PhCs, and metal gratings for the layer of SWS. Figure 2 is the sketch of the PG-SWC with the cylinders of the 2D PhCs dotting on the cross-section of the SWC. In Fig.2, the z-direction is the direction of the power flowing. If the metal gratings extend into the layer of PhCs as shown in Fig.3, it turns into

*Project supported by the National Natural Science Foundation of China (Grant Nos 60532010 and 60601005).
†E-mail: yhr555@sohu.com

that made by the preferential technology presented in Ref.[3]. In these PG-SWCs, the metal gratings are both for generating slow EMW and for supporting wiggler magnets. The ribbon beam will have an aspect ratio of 1 to 10, which effectively lowers the beam perveance by a factor of 10 in comparison with that of a circular beam. Correspondingly, the efficiency is expected to be higher, while the fabrication cost will be lower.

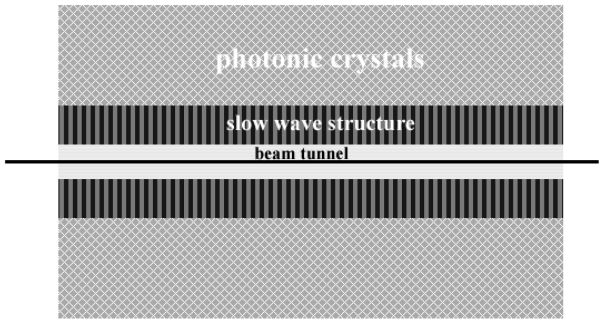


Fig.1. The schematic diagram of theoretical PhC SWCs.

Chen *et al*[6] have presented a simplified method of analysing the PG-SWC. In this method, the PG-SWC is assumed to extend in the x-direction infinitely, so only the TM polarization of the PhCs is calculated in their analysis. But this assumption cannot hold true in reality. When the PG-SWC extension in x-direction is not infinite, the polarization is another story, so is the photonic band gap (PBG) of this polarization. As the operating band is determined by the PBG of the PhC, the excursion of the PBG obtained under the assumption of infinity will lead to the design failure. In this paper, the method of analysing the practical PG-SWC is considered, and the procedure of design is explained by two examples.

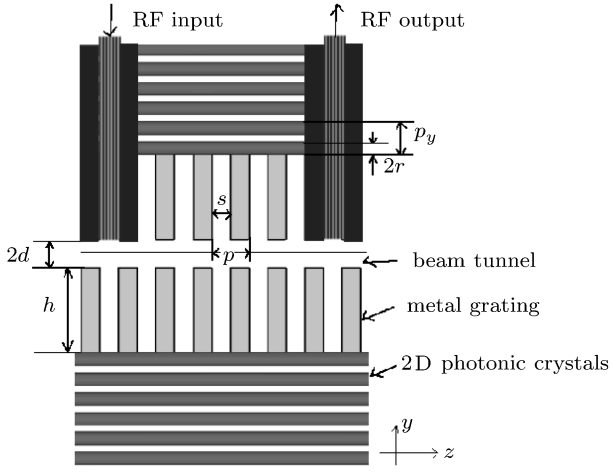


Fig.2. The sketch of PG-SWC.

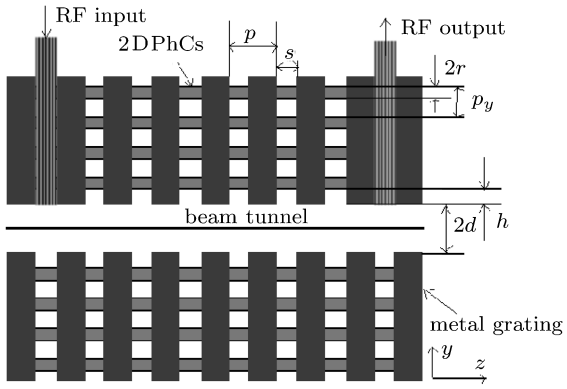


Fig.3. The sketch of PG-SWC with gratings extending into the layer of PhCs.

2. Theory

The dimensional parameters of the PG-SWC have been marked in Figs.2, 3 and 4. In the following, these parameters will be directly used.

A well designed PG-SWC should completely reflect the EMW of the operating mode. For the operating mode confined within the layers of SWS and beam tunnel, the PG-SWC acts as a rectangular waveguide grating, with the height along the y-direction being $2(b+h)+\delta$. Here, δ is very small, and equal to the penetration depth of the EMW. Correspondingly, the analysis can be implemented by two steps: calculating the band-structures for the 2D PhC, and analysing the dispersion for the equivalent rectangular waveguide grating. In the following, the band-structures of the PhCs will be studied first.

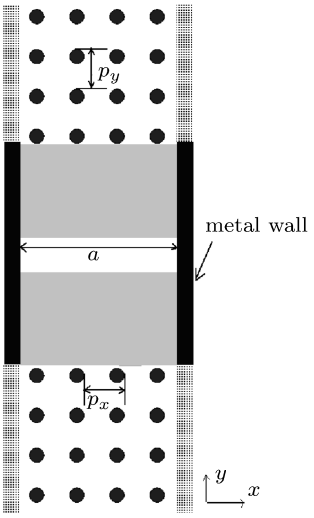


Fig.4. The $x-y$ plane view of PG-SWC.

In the systems shown in Figs.2 and 3, the incident EMWs upon the PhCs can be classified as TE and TM polarizations. As the incident TE and TM modes can propagate along the z-direction, and the structure is enclosed by two metal walls along the x-direction, the incident TE and TM modes here are slightly different from the purely TE and TM polarizations which are commonly used in the analysis of infinitely extending 2D PhCs. Here, the incident TE and TM modes are not homochromatic plane waves along the z-direction, and can be viewed as the superposition of homochromatic plane waves. In the following, the eigenvalue equations of the TE and TM polarizations will be derived successively by plane wave method (PWM).[7]

2.1. TE polarization

In the case of TE polarization, the EM fields have the forms

$$\boldsymbol{E} = [E_x,\ E_y,\ 0]\exp(\mathrm{j}\omega t), \tag{1a}$$

$$\boldsymbol{H} = [H_x,\ H_y,\ H_z]\exp(\mathrm{j}\omega t). \tag{1b}$$

The Maxwell curl equations for the above field components are

$$\frac{\partial H_x}{\partial y} - \frac{\partial H_y}{\partial x} = 0, \tag{2a}$$

$$\frac{\partial H_z}{\partial x} - \frac{\partial H_x}{\partial z} = \mathrm{j}\omega\varepsilon_\mathrm{f}[1-(1-\varepsilon_\mathrm{r})S_{(x,y)}]E_y, \tag{2b}$$

$$\frac{\partial H_y}{\partial z} - \frac{\partial H_z}{\partial y} = \mathrm{j}\omega\varepsilon_\mathrm{f}[1-(1-\varepsilon_\mathrm{r})S_{(x,y)}]E_x, \tag{2c}$$

$$\frac{\partial E_x}{\partial y} - \frac{\partial E_y}{\partial x} = -\mathrm{j}\omega u_0 H_z, \tag{2d}$$

$$-\frac{\partial E_x}{\partial z} = -\mathrm{j}\omega u_0 H_y, \tag{2e}$$

$$\frac{\partial E_y}{\partial z} = -\mathrm{j}\omega u_0 H_x. \tag{2f}$$

Eliminating all the elements of H gives the following equations:

$$\nabla^2 E_x + k^2 E_x - k^2(1-\varepsilon_\mathrm{r})S_{(x,y)}E_x = 0, \tag{3}$$

$$\nabla^2 E_y + k^2 E_y - k^2(1-\varepsilon_\mathrm{r})S_{(x,y)}E_y = 0. \tag{4}$$

where ε_f is the permittivity of the background material in the layer of PhCs. $\varepsilon_\mathrm{r} = \varepsilon_\mathrm{p}/\varepsilon_\mathrm{f}$, ε_p is the permittivity of the PhCs. $S_{(x,y)}$ is a periodic function with the periodicity of the PhC reciprocal Bravais lattice. $S_{(x,y)} = 1$, if the field point is inside the cross-section of the PhC cylinders, and $S_{(x,y)} = 0$, if the point is outside the cross-section of the PhC cylinders.

From expressions (2), the field components of E_x and E_y can be expressed mutually, thus, solving Eq.(3) or (4) is enough. The E_x can be written as the following form:

$$E_x^{(\mathrm{p})} = \sum_{l,m,n} A_{l,m,n}\exp\Big[\mathrm{j}\Big(k_x + \frac{2l\pi}{p_x}\Big)x + \mathrm{j}\Big(k_y + \frac{2m\pi}{p_y}\Big)y\Big]F_{n(z)}, \tag{5}$$

where k_x and k_y are the transmission constants along the x- and y-directions, respectively. For Fig.2

$$F_{n(z)} = \exp(\mathrm{j}\beta_n z), \tag{6}$$

where $\beta_n = \beta_0 + 2n\pi/p$, β_0 is the same transmission constant as that in the beam tunnel. For Fig.3 we have

$$F_{n(z)} = \delta_{(z,s)}\cos\Big[\frac{n\pi(z-wp)}{s}\Big], \tag{7}$$

where w is an integer, and $\delta_{(z,s)}$ is a delta function, which is equal to 0 when z is in the gratings, and equal to 1 when z is out of the gratings.

The function $S_{(x,y)}$ can be expanded as a Fourier series:

$$S_{(x,y)} = \sum_{l=-\infty}^{\infty}\sum_{m=-\infty}^{\infty} G_{l,m}\exp\Big[\mathrm{j}2\pi\Big(\frac{l}{p_x}x + \frac{m}{p_y}y\Big)\Big]. \tag{8}$$

When expressions (5)–(8) are substituted into Eq.(3), the eigenvalue equation will be given as the equation satisfied by the coefficient $A_{l,m,n}$

$$k^2(1-\varepsilon_\mathrm{r})\sum_{l'}\sum_{m'} A_{l',m',n}G_{l-l',m-m'} = \Big[k^2 - \Big(k_x + \frac{2l\pi}{p_x}\Big)^2 - \Big(k_y + \frac{2m\pi}{p_y}\Big)^2 - \xi_n^2\Big]A_{l,m,n}, \tag{9}$$

where $k = \omega\sqrt{\varepsilon_\mathrm{f}}/c$, and c is the speed of light in vacuum; $\xi_n = \beta_n$ in Fig.2, and $\xi_n = n\pi/s$ in Fig.3. If the PG-SWC is enclosed by two metal walls as shown in Fig.4, $k_x = v\pi/a$, v is an integer larger than zero, which is equal to the index number of the modes of the rectangular waveguide grating.

2.2. TM polarization

In the case of TM polarization, the EM fields have the forms

$$\boldsymbol{E} = [E_x,\ E_y,\ E_z]\exp(\mathrm{j}\omega t), \tag{10a}$$

$$\boldsymbol{H} = [H_x,\ H_y,\ 0]\exp(\mathrm{j}\omega t). \tag{10b}$$

The Maxwell curl equations for the above field components are

$$\frac{\partial E_x}{\partial y} - \frac{\partial E_y}{\partial x} = 0, \tag{11a}$$

$$\frac{\partial E_z}{\partial x}-\frac{\partial E_x}{\partial z}=-\mathrm{j}\omega u_0 H_y, \tag{11b}$$

$$\frac{\partial E_y}{\partial z}-\frac{\partial E_z}{\partial y}=-\mathrm{j}\omega u_0 H_x, \tag{11c}$$

$$\frac{1}{\varepsilon_\mathrm{f}}\Big[1-\Big(1-\frac{1}{\varepsilon_\mathrm{r}}\Big)S_{(x,y)}\Big]\Big(\frac{\partial H_x}{\partial y}-\frac{\partial H_y}{\partial x}\Big)=\mathrm{j}\omega E_z, \tag{11d}$$

$$-\frac{1}{\varepsilon_\mathrm{f}}\Big[1-\Big(1-\frac{1}{\varepsilon_\mathrm{r}}\Big)S_{(x,y)}\Big]\frac{\partial H_x}{\partial z}=\mathrm{j}\omega E_y, \tag{11e}$$

$$\frac{1}{\varepsilon_\mathrm{f}}\Big[1-\Big(1-\frac{1}{\varepsilon_\mathrm{r}}\Big)S_{(x,y)}\Big]\frac{\partial H_y}{\partial z}=\mathrm{j}\omega E_x. \tag{11f}$$

Eliminating all the elements of E yields the following equation:

$$\frac{1-\varepsilon_\mathrm{r}}{\varepsilon_\mathrm{r}}\nabla\bullet S_{(x,y)}\nabla H_x+\nabla^2 H_x+k^2 H_x=0. \tag{12}$$

The H_x can be written as follows:

$$H_x^{(\mathrm{p})}=\sum_{l,m,n}B_{l,m,n}\exp\Big[\mathrm{j}\Big(k_x+\frac{2l\pi}{p_x}\Big)x+\mathrm{j}\Big(k_y+\frac{2m\pi}{p_y}\Big)y\Big]H_{n(z)}. \tag{13}$$

For Fig.2,

$$H_{n(z)}=\exp(\mathrm{j}\beta_n z). \tag{14}$$

For Fig.3,

$$F_{n(z)}=\delta_{(z,s)}\sin\Big[\frac{n\pi(z-wp)}{s}\Big]. \tag{15}$$

When expressions (13)–(15) are substituted into Eq.(12), the eigenvalue equation of the TM polarization is as follows:

$$\begin{aligned}&\frac{1-\varepsilon_\mathrm{r}}{\varepsilon_\mathrm{r}}\sum_{l'}\sum_{m'}B_{l',m',n'}G_{l-l',m-m'}\\&\times\Big[\Big(k_x+\frac{2l\pi}{p_x}\Big)\Big(k_x+\frac{2l'\pi}{p_x}\Big)\\&+\Big(k_y+\frac{2m\pi}{p_y}\Big)\Big(k_y+\frac{2m'\pi}{p_y}\Big)+\xi_n\xi_n'\Big]\\&=\Big[k^2-\Big(k_x+\frac{2l\pi}{p_x}\Big)^2-\Big(k_y+\frac{2m\pi}{p_y}\Big)^2-\xi_n^2\Big]B_{l,m,n}.\end{aligned} \tag{16}$$

2.3. The dispersion equation of the equivalent rectangular waveguide grating SWC

As discussed above, the PG-SWC is equivalent to a rectangular waveguide grating SWC for the modes inside the PBG of the PhCs. As the penetration depth is small, it can be neglected. Thus, following the way in Ref.[8], the fields are expanded in terms of spatial eigenfunctions, and the boundary conditions at the interfaces are imposed to interrelate the coefficients of each eigenfunction expansion. Then, the eigenvalue equation can be expressed as

$$\sum_{n'=-\infty}^{\infty}A_{n'}X_{n,n'}=A_n\frac{F_n'(0)L}{k_0^2-(v\pi/a)^2} \tag{17}$$

with

$$X_{n,n'}=\frac{2F_{n'}(0)}{s}\sum_{m=0}^{\infty}\frac{G_m'(0)\int_0^s\cos(m\pi z/s)\exp(-\mathrm{j}\beta_n z)\mathrm{d}z\int_0^s\cos(m\pi z/s)\exp(\mathrm{j}\beta_n z)\mathrm{d}z}{[k_0^2-(v\pi/a)^2]G_m(0)(1+\delta_{m0})}, \tag{17a}$$

$$F_n(y)=\begin{cases}\cos|\gamma_n|(h-y), & \gamma_n^2=k_0^2-(l\pi/a)^2-\beta_n^2>0,\\ \cosh|\gamma_n|(h-y), & \gamma_n^2=k_0^2-(l\pi/a)^2-\beta_n^2<0,\end{cases} \tag{17b}$$

$$F_n'(y)=\frac{\partial F_n(y)}{\partial y}, \tag{17c}$$

$$G_m(y)=\begin{cases}\cos[|\tau_m|(y+h)], & \tau_m^2=k_0^2-(l\pi/a)^2-(m\pi/s)^2>0,\\ \cosh[|\tau_m|(y+h)], & \tau_m^2=k_0^2-(l\pi/a)^2-(m\pi/s)^2>0,\end{cases} \tag{17d}$$

$$G_n'(y)=\frac{\partial G_n(y)}{\partial y}, \tag{17e}$$

$$k_0^2=\omega^2\varepsilon_0 u_0, \tag{17f}$$

where δ_{m0} is the Kronecker delta function, v being an integer, which is equal to the index number of mode along the x-direction.

The eigenfrequencies obtained from Eq.(17) do not exist in practice except those that are inside the PBGs of the corresponding polarization of the PhCs. This is important and worth being pointed out again.

3. Numerical calculations

Firstly, we consider the case as shown in Fig.3 where the 2D PhCs are not enclosed by two metal walls. The dimensional parameters of the 2D PhCs for the calculation are given in Table 1. In the following

calculation, the width of the SWS layer, a, is assumed to be definite; and the cylinders of the 2D PhCs are assumed to be cuboids in shape. In Table 1, d_x and d_y are the lengths of the PhC cylinders along the x- and the y-directions, respectively; e_b and e_c are the relative permittivities of the background material and the PhC cylinders, respectively; the other two dimensional parameters are shown in Fig.4. As the PhCs are not enclosed by metals walls, Eqs.(9) and (16) do not include the index number of the incident waves (the waves in the layers of SWS and beam tunnel), and the k_x and k_y can be an arbitrary value between 0 and π/p_x and between 0 and π/p_y, respectively. The band-structures of the TE and TM polarizations in this case are shown in Figs.5 and 6, respectively.

Table 1. The parameters in analysing 2D PhCs.

name	value	name	value
p_x/a	0.14	p_y/a	0.14
d_x/a	0.07	d_y/a	0.07
e_b	16.5	e_c	3

As can be seen from Figs.5 and 6, there are a PBG of the TE polarization inside the band of $1.43289 \sim 1.67785$ and a PBG of the TM polarization inside the band of $1.29866 \sim 1.55705$. As the incident wave may be of TE polarization, or TM polarization, or the blend of TE and TM polarization, only the wave inside the collective PBG of TE and TM polarizations can be confined and propagate along the z-direction definitely in the layers of the SWS and in the beam tunnel. The collective PBG of the TM and TE polarizations is $1.43289 \sim 1.55705$. The collective PBG chiefly determines the operating band-width of the PG-SWC TWTs.

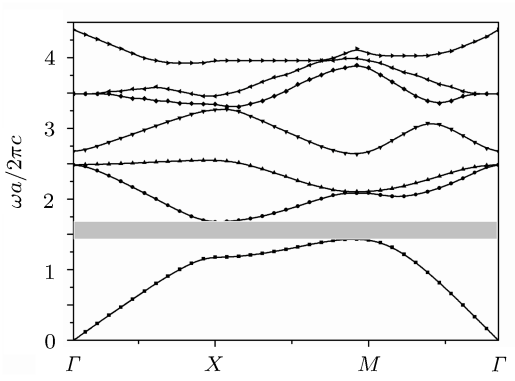


Fig.5. The band-structure of the TE polarization of the 2D PhCs in the system shown in Fig.3.

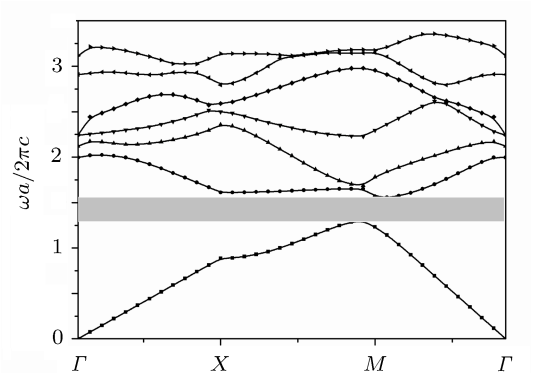


Fig.6. The band-structure of the TM polarization of the 2D PhCs in the system shown in Fig.3.

The operating mode is designed inside the collective PBG in an approximate way of Eq.(17). The design results are shown in Figs.7 and 8, where the dimensional parameters are optimized when a tradeoff is maintained between the phase speed and band-width. The dimensional parameters are shown in Table 2. In Fig.8, the mode of $\mathrm{TE}_{x(11)}$ is the lowest anti-symmetry mode, while the mode of $\mathrm{TE}_{x(12)}$ is the lowest symmetry mode. As the symmetry modes can be eliminated by introducing a continuous conducting sheet on the symmetry axis of the system,[9] the effect of the symmetry mode is not considered here. In Fig.7, the band covered by slanting lines is the collective PBG of the TE and TM polarizations of the PhCs in the system; the band between the two solid lines is the operating band when the tuning voltage is in the range of 5%.

Table 2. The dimensional parameters of the layers of SWS and beam tunnel for the cases of Figs.7 and 8.

name	value	name	value
p/a	0.1	s/a	0.07
h/a	0.1	d/a	0.03

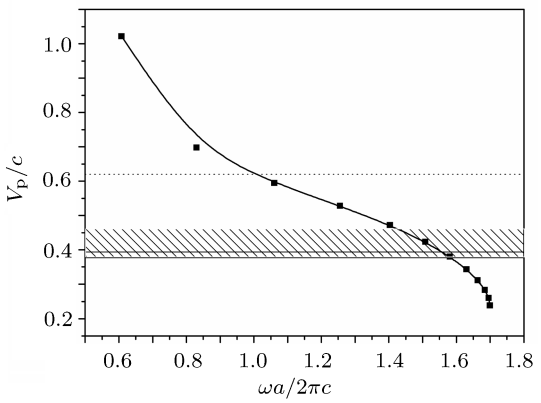


Fig.7. The diagram of phase speed versus frequency of the TE_{11} mode of the equivalent SWS in the system shown in Fig.3.

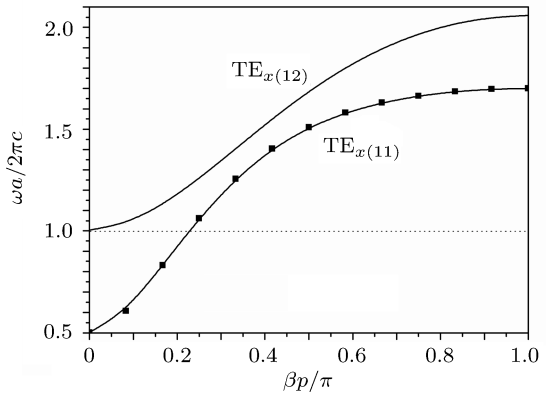


Fig.8. The diagram of phase shift versus frequency of the TE_{11} and TE_{12} modes of the equivalent SWS in the system shown in Fig.3.

To validate the above design, the scattering parameters of the lowest anti-symmetry mode are calculated. During the calculation, three grating pitches are assumed to exist in the z-direction, seven PhC pitches along the x-direction, and two PhC pitches along the y-direction; the boundaries normal to the x-direction are enclosed by conductive walls, and the boundaries normal to the y-direction are set to be periodic; the boundaries normal to the z-direction are set to be open. Computer Simulation Technology Microwave Studio (CST MWS) is used in this calculation. The ports are located in the boundary plane along the z-direction. The iterative accuracy is set to be -80 dB, and 2506738 grids are used. The convergence accuracy is 1×10^{-6}. Figure 9 shows the amplitude of the scattering parameter of S_{12}. The incidence phase is switched to 90 degree. As can be seen from Fig.9, there exists a complete transmission band of $1.431 \sim 1.572$. This band has little difference from that for the collective PBG of $1.43289 \sim 1.55705$. The good accordance between the complete transmission band and the collective PBG implies that the design method provided by this paper is correct and the error is small.

For the system with a circuit shown in Fig.2, from Eqs.(9) and (16), the band structures of the PhCs are determined by a wave vector of $k_x\boldsymbol{x}+k_y\boldsymbol{y}+\beta_0\boldsymbol{z}$ when the layer of PhCs is not enclosed by metal walls. There are three transmission constants, so the calculation is complex. To simplify the calculation, it is assumed that the PhC layer is enclosed by two metal walls along the x-direction. The width of the layer of PhCs along the x-direction is assumed to equal the width of the layers of SWS and beam tunnel as shown in Fig.4. In this case, the transmission constant of k_x is equal to $v\pi/a$, where v is the integer of the mode index number in Eq.(17). As the mode index number is included in the eigenvalue equations of the PhCs, the PBG of a mode with a definite mode index number has a possibility for it to be completely separated from the PBG of another mode with a different mode index number when the PhCs are optimized. Thus, the introduction of confining metal walls will benefit the design of the PG-SWC.

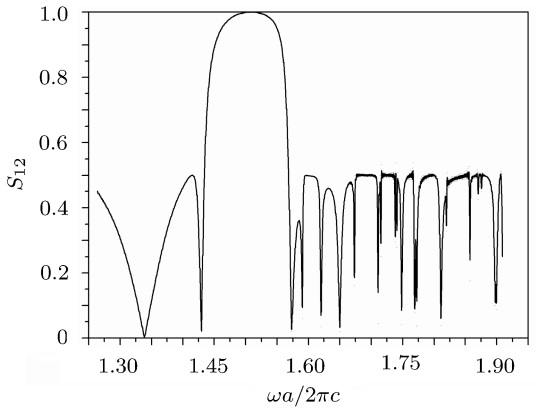


Fig.9. The S_{12} of the lowest anti-symmetry mode for the system shown in Fig.3.

The band-structures of the TE_{1n} polarization and TM_{1n} polarization are shown in Figs.10 and 11, respectively. For the calculation results of Figs.10 and 11, the parameters of the PhCs are the same as those shown in Table 1. Because the PhCs are enclosed by two metal walls, the lower cutoff eigenfrequencies in Figs.10 and 11 are not zeros. As can be seen from Figs.10 and 11, there exists no PBG no matter whether the incidence wave is of TE_{1n} polarization or TM_{1n} polarization for the enclosed PhCs. The reason why no PBG exists is that the wave is incident upon the 2D PhCs from the $x-z$ plane, whereas the 2D PhCs is symmetry in that plane. That is why there exists a non-zero transmission constant of β_0.

In Figs.10 and 11, $\beta_0 p$ is zero in the region from Γ to X on the horizontal axis, and varies from zero to π in the region from X to M, then varies from π to zero in the region from M to Γ. Though no PBG exists in the cases of Figs.10 and 11, the pass-band interval can be non-zero between two different values of β_0. For example, there is a pass-band interval of 1.498–1.575 when $\beta_0^* p$ varies from 0 to $\pi/4$ as shown in Fig.11. As the wave in the layer of beam tunnel and the wave in the layer of PhCs share the same transmission constant along the z-direction, the wave can be confined in the layers of beam tunnel and SWS, if

the wave has a transmission constant β_0 between its upper and bottom boundaries for the pass-band interval, and an eigenfrequency is inside the pass-band interval.

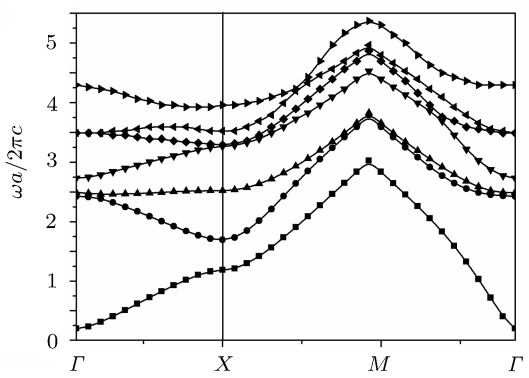


Fig.10. The band-structure of the TE_{1n} polarization of the 2D PhCs in the system shown in Fig.2.

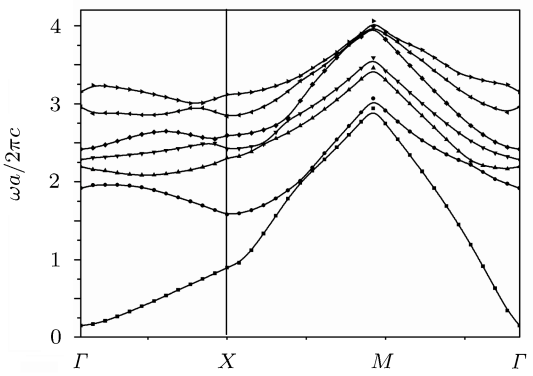


Fig.11. The band-structure of the TM_{1n} polarization of the 2D PhCs in the system shown in Fig.2.

The shadowed area in Fig.12 is the collective pass-band interval of the TE_{1n} polarization and the TM_{1n} polarization, and the pass-band of the TE_{11} mode. Inside the shadowed area, the value of $\beta_0 p$ varies from 0.0856 to 0.1645. Figure 13 is the diagram of the phase speed versus the eigenfrequency of the TE_{11} mode. For this TE_{11} mode, the dimensional parameters of the layers of SWS and beam tunnel are listed in Table 3. In Fig.12, the area covered by slanting lines is the collective pass-band interval of the TE_{1n} polarization and the TM_{1n} polarization when the value of $\beta_0 p$ varies from 0.0856 to 0.1645 shown in Fig.12. The band between the two solid lines is the operating band when the range of tuning voltage is within 5%.

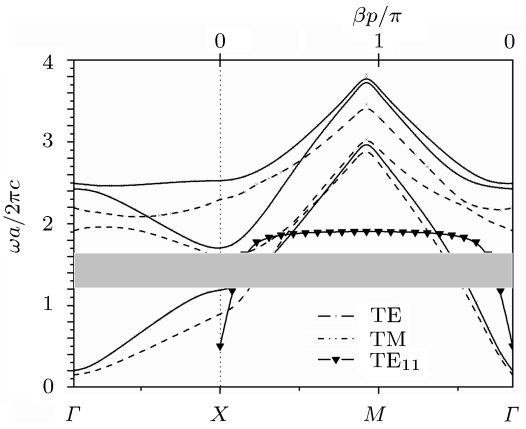


Fig.12. The collective pass-band interval of the TE_{1n} and TM_{1n} polarizations for the 2D PhCs and the dispersion of the TE_{11} mode in the system shown in Fig.2.

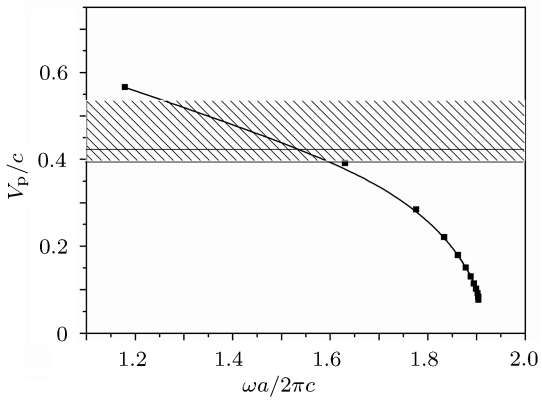


Fig.13. The diagram of phase speed versus frequency of the TE_{11} mode of the equivalent SWS in the system shown in Fig.2.

Table 3. The dimensional parameters of the layers of SWS and beam tunnel for the case of Fig.14.

name	value	name	value
p/a	0.025	s/a	0.015
h/a	0.06	d/a	0.03

Though the methods of the systems shown in Figs.2 and 3 are the same, the band structures of the PhCs in Fig.2 are distinct from those in Fig.3. In Fig.2, there is no PBG existing for the wave which is incident upon the PhCs with an arbitrary value of β_0. As the possible operating band of the PG-SWC TWTs is inside the pass-band interval limited by the transmission constant along the z-direction, the design of the layers of SWS and beam tunnel is little flexible in comparison with the design of the system shown in Fig.3.

4. Conclusions

The eigenvalue equations of the PhCs are derived corresponding to the special polarizations of the wave in the PG-SWC. Two design examples are given. The possible operating band of the PG-SWC TWTs shown in Fig.3 is inside the collective PBG of the TM polarization and the TE polarization, when the PhCs are not enclosed by metal walls and extend infinitely. For the TWTs based on the PG-SWC shown in Fig.2, the possible operating band is inside the collective pass-band interval of the TM_{1n} polarization and TE_{1n} polarization, when the PhCs are enclosed by two metal walls located along the x-direction. For the PG-SWC shown in Fig.2, only a portion of the pass-band of the operating mode, in which eigenfrequencies are inside the collective pass-band interval and the transmission constant is between the upper and bottom boundaries of the collective pass-band interval, can propagate along the z-direction and cannot leak out of the PhCs. This requirement makes the design of layers of SWS and beam tunnel of Fig.2 less flexible than that of the system in Fig.3.

References

[1] Slater J 1950 *Microwave Electronics* (New York: Van Nostrand) p5

[2] Yablonovich E and Gmitter T J 1986 *Phys. Rev. Lett.* **63** 1950

[3] He B L, Liu P K and Tang C J 2006 *Acta Phys. Sin.* **55** 1862 (in Chinese)

[4] Gong Y B, Zhang Z, Wei Y Y and Wang W X 2004 *Acta Phys. Sin.* **53** 3990 (in Chinese)

[5] Lu Z G, Gong Y B, Wei Y Y and Wang W X 2006 *Acta Phys. Sin.* **55** 3590 (in Chinese)

[6] Chen C P, Qian B L and Temkin J R 2005 *Photonic Crystal Ribbon-Beam Traveling Wave Amplifier* (Boston: United States Patent Application Publication)

[7] Plihal M and Maradudin A A 1991 *Phys. Rev.* B **44** 8565

[8] Maragos A A, Ioannidis Z C and Tigelis I G 2003 *IEEE Trans. on Plasma Science* **31** 1075

[9] Freund H P and Abu-Elfadl T M 2004 *IEEE Trans. on Plasma Science* **32** 1015